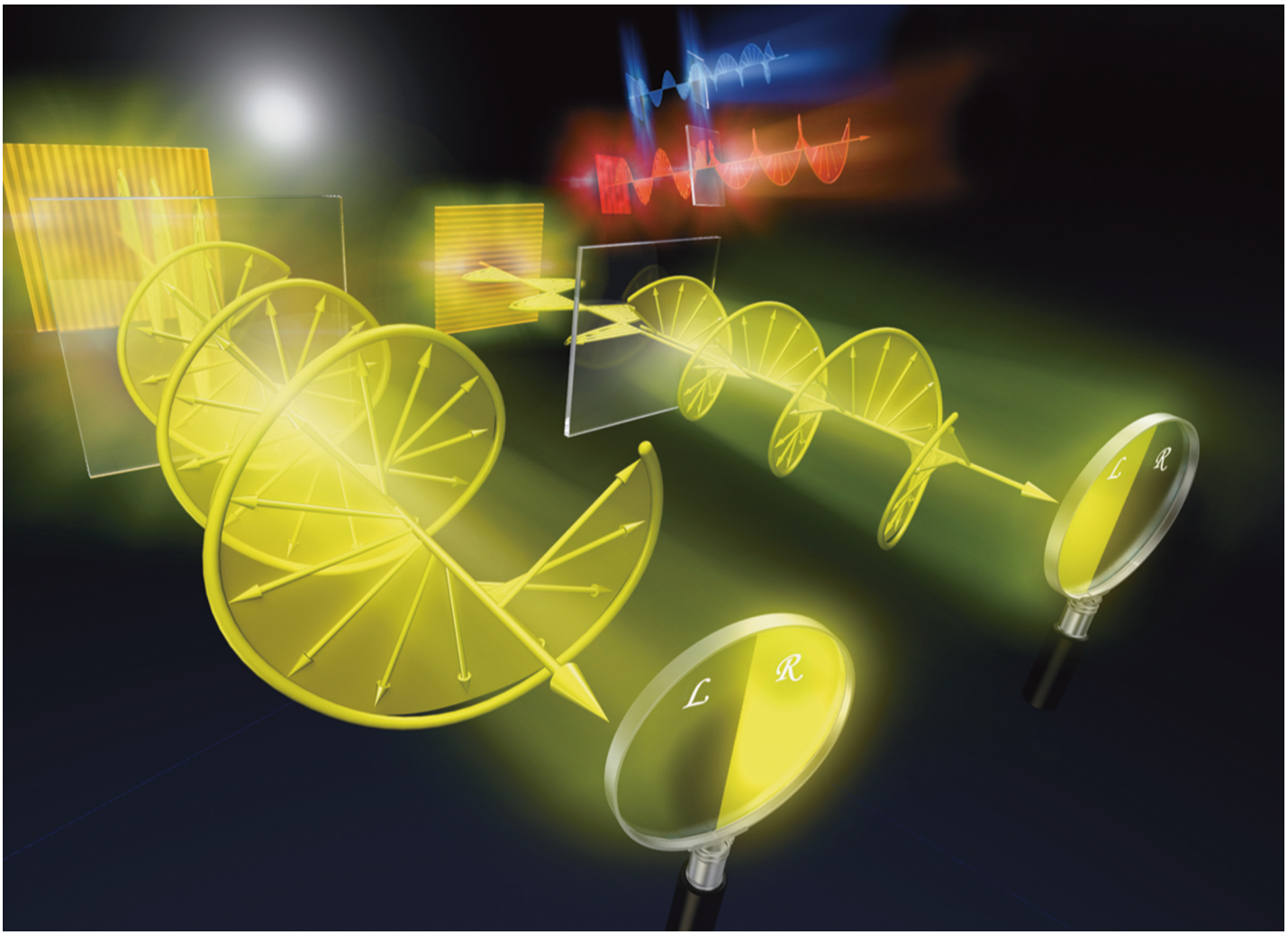

Showcasing research from Dr Yutaka Okazaki, Graduate School of Energy Science, Kyoto University, Kyoto, Japan.

Luminescence-based circular polarization convertors: polarization conversion of linearly polarized photoluminescence from one-dimensionally aligned quantum rods using retardation films

Generation of circularly polarized (CP) light with high purity and light intensity was achieved by single-, parallel, and multi-layered luminescence-based CP convertors composed of linearly polarized luminescence (LPL) films and quarter-wave plate.

As featured in:

See Yutaka Okazaki, Takashi Sagawa *et al.*, *J. Mater. Chem. C*, 2023, **11**, 935.

ROYAL SOCIETY OF CHEMISTRY

rsc.li/materials-c

Registered charity number: 207890

Journal of Materials Chemistry C

ROYAL SOCIETY OF CHEMISTRY

PAPER

View Article Online
View Journal | View Issue

Check for updates

Cite this: J. Mater. Chem. C, 2023, 11, 935

Luminescence-based circular polarization convertors: polarization conversion of linearly polarized photoluminescence from one-dimensionally aligned quantum rods using retardation films†

Yutaka Okazaki, * Misaki Kimura, Kan Hachiya and Takashi Sagawa *

Received 20th September 2022,
Accepted 10th November 2022

DOI: 10.1039/d2tc03955a

rsc.li/materials-c

Existing methods for generating circularly polarized (CP) light from an unpolarized light source without using external electrical energy have drawbacks, such as a trade-off relationship between CP light intensity and purity. Here, we demonstrate an approach for the generation of high-purity, high-intensity CP light based on a luminescence-based CP convertor composed of a linearly polarized luminescence (LPL) film and a quarter-wave plate. The LPL films, fabricated by one-dimensional alignment of semiconductor quantum rods and laminated with a quarter-wave plate, enabled effective conversion of LPL to high-purity CP light and retained the photoluminescent spectral pattern, light intensity, and the large degree of polarization. The sign of CP light was easily switched by changing the orientation of the quarter-wave plate and the LPL polarization plane. Furthermore, we also demonstrate the first example of parallel-type and multi-layered luminescence-based CP light convertors for multiplexing optical information. Our findings will aid the design of next-generation CP light-generating materials.

Introduction

Circularly polarized (CP) visible light is gathering worldwide attention as a next-generation light source because it exhibits extensive optical information, a wide viewing angle, and asymmetric effects, such as chiral induction,[1] enantioselective chemical reactions,[2,3] and enhancement of the energy conversion efficiency of photovoltaics (inverse Faraday effect).[4] In recent years, the improvement of various optical properties, such as the polarization degree, light intensity, and color tunability, has been considered an important issue in the generation of CP light. The majority of the reported approaches for creating CP visible light from unpolarized light without using external electrical energy can be roughly classified into three categories, namely, filtration using a circular polarizer, selective reflection by chiral liquid crystal structures,[5] and circularly polarized luminescence (CPL) from chiral materials.[6] A classical filtering method using a circular polarizer made from a linear polarizer and quarter-wave plate has been widely used, especially in the field of optics, because it can produce high-purity CP light with high reliability. A selective reflection method using chiral liquid crystal structures, which is based on biomimetics,[7] can also produce high-purity CP light with unique properties, such as angular dependence of color (structural color) owing to Bragg's law. Another unique property of this approach is that CP transmitted light has an opposite signal to that of CP reflected light. The significantly high polarization degree of CP light obtained from the above two methods originates from the precise filtration or separation of the one-sided CP light, resulting in a theoretical light intensity limitation of less than 50%. In contrast to the above two approaches, the CPL approach allows various highly emissive CP luminophores exhibiting various emission colors to be selected. However, the quantum yield (ϕ), indicating luminescence intensity, and the dissymmetry factor (g_{lum}), indicating the polarization degree of CP light upon luminescence, are generally in a trade-off relationship.[8] Therefore, despite remarkable recent progress in CP light generation, the creation of high-purity CP visible light with high light intensity remains an important challenge.

Linearly polarized luminescence (LPL), on the other hand, has no theoretical constraints in achieving both high polarization degree and high light intensity. Various approaches have been reported for the fabrication of LPL materials, including

Graduate School of Energy Science, Kyoto University Yoshida-Honmachi, Sakyo-ku, 606-8501 Kyoto, Japan. E-mail: okazaki.yutaka.8c@kyoto-u.ac.jp, sagawa.takashi.6n@kyoto-u.ac.jp

† Electronic supplementary information (ESI) available. See DOI: https://doi.org/10.1039/d2tc03955a

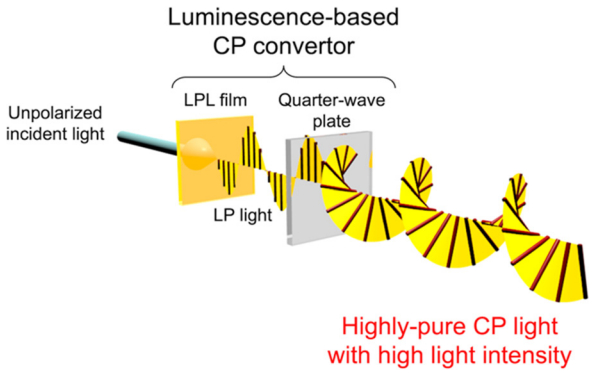

Fig. 1 Schematic illustration of high-purity CP visible light generation by conversion of LPL.

stretching,[9a] the fiber-directed method,[9b] shearing,[9c–e] rubbing,[9f] evaporation,[9g,h] the Langmuir–Blodgett method,[9i,j] external field,[9k] and photo-induction.[9l–n] However, effective use of LPL films for producing high-purity CP visible light with high light intensity, has not been investigated so far, not to mention the effect of multilayering of LPL films.

Here, we demonstrate an approach based on the polarization conversion of LPL to produce high-purity CP visible light with high light intensity (Fig. 1). This approach enables various achiral photoluminescent (PL) dyes to be selected. Therefore, the emission color and light intensity can be easily tuned using the PL spectra and quantum yield of dyes. By laminating a quarter-wave plate on the LPL material, the polarization degree of LPL is directly converted to the polarization degree of CP light (P_{CP}), resulting in an extremely large P_{CP} value. The sign (right-handed (RH) or left-handed (LH)) of CP light can be easily switched with retention of the PL spectral pattern and intensity by simply changing the angle between the fast axis of the quarter-wave plate and polarization plane of LPL from +45° to −45° (or from −45° to +45°).

In comparison with a circular polarizer, a luminescence-based CP convertor uses a LPL film instead of a linear polarizer. The most significant difference between LPL films and linear polarizers is the spectral conversion properties derived from the photoluminescent phenomenon. Taking advantage of spectral conversion properties of LPL films, LP light at desired wavelength can be produced from incident light at undesired wavelength. From the viewpoint of energy loss, when unpolarized light at desired wavelength is filtered by a linear polarizer, more than half of light energy is cut off. In contrast, in the case of LPL films, the emitted light at desired wavelength is already highly polarized. Therefore, light energy loss can be prevented by using LPL films, even when combined with a linear polarizer. Further advantage of this approach can be found in the multilayering of LPL films. Details will be given later.

In the present paper, LPL films were fabricated by the one-dimensional alignment of semiconductor quantum rods (QRs) with the following advantages: (i) LPL can be generated along the long axis of nanorods; (ii) a high molar coefficient and quantum yield are obtained, which lead to a high light intensity; (iii) a sharp PL peak; and (iv) various QRs with different emission colors can be excited at one selected wavelength by taking advantage of the semiconductor features. The latter two features are key properties for the multiplexing of optical information from a CP light convertor. Herein, we demonstrate that our luminescence-based CP conversion approach provides high-purity CP light that is easily detected by the naked eye using a circular polarizer. We also demonstrated switching of the sign of CP light by simply changing the angle between the fast axis of the quarter-wave plate and polarization plane of LPL, and multiplexing of the optical information using parallel-type and multilayered luminescence-based CP light convertors.

Results and discussion

In this study, CdSe/CdS core/shell QRs were selected because the emission color can be easily tuned by selecting the size of the CdSe core particles. CdSe/CdS core/shell QRs were synthesized by the hot-injection method (see ESI†).[10] When CdSe quantum dots showing different emission colors were used as core particles (Fig. S1–S3, ESI†), the obtained solutions showed yellow-, orange-, and red-colored emission under UV light irradiation, respectively (Fig. 2a–c). Fig. 2d shows UV-vis and PL spectra of these three solutions. UV-vis spectra of yellow-, orange-, and red-QRs showed clear first absorption peaks at 573, 593, and 610 nm, respectively, corresponding to the energy gap between the valence and conduction bands of the CdSe core. The broad absorption bands below 500 nm, which were attributed to energy gaps between the valence and conduction bands of the CdS shell, were observed from all three solutions. In the PL spectral measurements, sharp emission peaks were observed at 587 nm (FWHM = 22 nm) from yellow-QRs, 607 nm (FWHM = 29 nm) from orange-QRs, and 627 nm (FWHM = 28 nm) from red-QRs, respectively. The QR morphologies were evaluated by transmission electron microscopy (TEM) observation. TEM images of the dried samples of the QR toluene solutions showed quite uniform rod-like nanostructures. To quantitatively analyze the morphology, the length and width of 200 nanorods in TEM images were measured. For the orange-QRs, the average length was 29.6 nm (σ = 2.4) and the average width was 4.9 nm (σ = 0.5), as shown in Fig. 2e and f. The morphologies of the yellow-QRs and red-QRs were also evaluated, as summarized in Fig. S4 and S5 (ESI†). The crystal structure of nanorods was evaluated by high-resolution TEM (HR-TEM) observation and from its fast Fourier transformation (FFT) pattern. As shown in Fig. 2g, clear periodic patterns were observed. Both top and bottom HR-TEM images show the same lattice spacing (3.4 Å) along the long axis of nanorods, which is in agreement with that of the (002) lattice planes of a hexagonal wurtzite-type CdS crystal (Fig. 2h).[10a,11,12a] This is consistent with a preferential growth of CdS shells along the *c*-axis of the wurtzite-type crystal structure without change in the diameter. Element mapping of the nanorods was conducted using scanning transmission electron microscopy–energy dispersive X-ray spectroscopy (STEM-EDX). As shown in Fig. 2i, Cd and S atoms were located homogeneously in nanorods, while Se atoms were

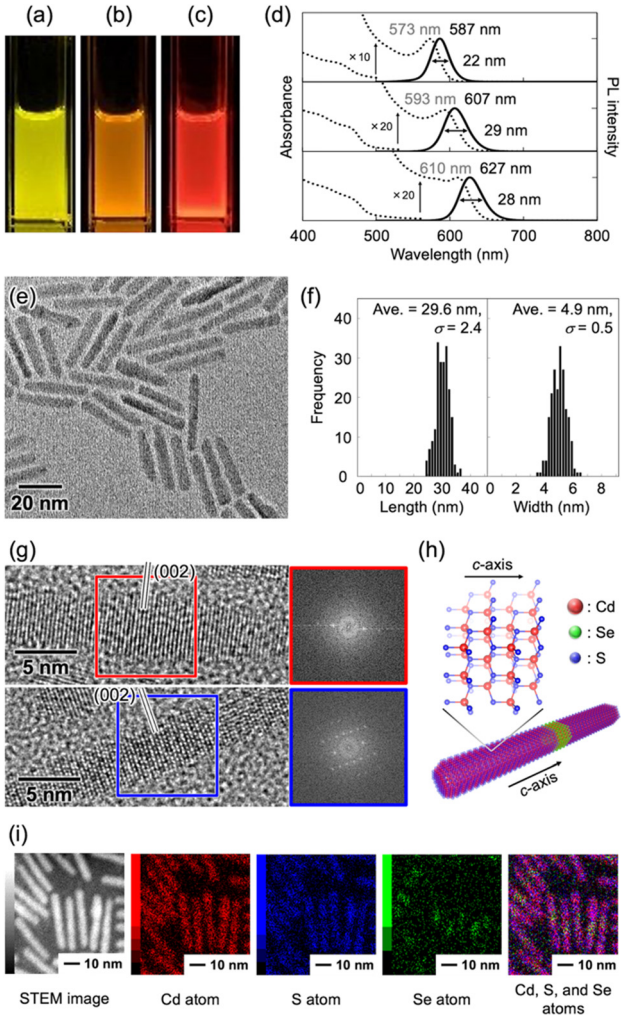

Fig. 2 (a–c) Photographs of QR toluene solutions showing (a) yellow-, (b) orange-, and (c) red-colored PL under UV light irradiation at 365 nm. (d) UV-vis (dotted lines) and PL (solid lines) spectra of yellow-, orange, and red-QRs suspended in toluene. All peak top PL intensities are adjusted to 1. (e) TEM image of orange-QRs. (f) Length (left) and width (right) distribution of orange-QRs. (g) HR-TEM images of orange-QRs. Insets show FFT patterns of the area selected by the red and blue squares. (h) Illustration of CdSe/CdS core/shell QRs and the hexagonal wurtzite-type CdS crystal. (i) STEM image (monotone) and element mapping (colored) of QRs. Red, blue, and green colors indicate Cd, S, and Se atoms, respectively.

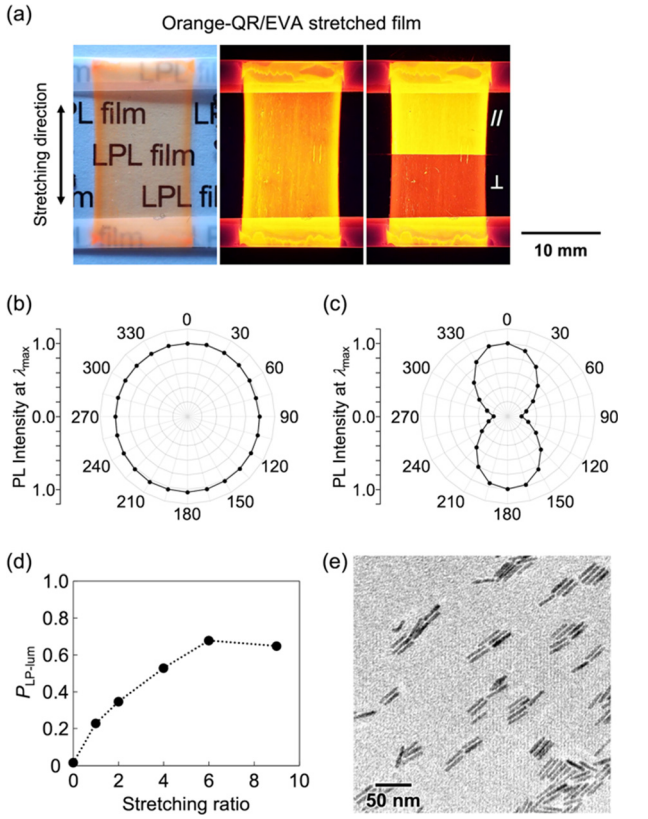

Fig. 3 (a) Photograph of 1D stretched orange-QR/EVA composite films taken under room light (left) and UV light at 365 nm (middle and right). In the case of right photographs, luminescence was observed through a linear polarizer placed in parallel (∥) and perpendicular (⊥) directions to the stretching direction. Angular dependence of PL intensity at λ_{max} of orange-QR/EVA composite films (b) before and (c) after 1D stretching. The stretching ratio was 7. (d) Plots of $P_{LP\text{-}lum}$ *versus* stretching ratio. (e) TEM images of orange-QR/EVA composite films after 1D stretching.

localized close to the center of the nanorods, confirming that the nanorods consisted of a CdS rod-like shell and CdSe core.

In general, the LPL properties of QRs significantly degraded in homogeneous bulk materials owing to their random orientation. To extract and maximize the LPL properties of QRs on the macroscale, the QRs were oriented in one direction (1D) by uniaxial stretching of the composite polymer films. In this study, we selected poly(ethylene-*co*-vinyl acetate) (EVA) as a stretchable polymer because of its transparency, elasticity, solubility, and adhesive properties on various substrates. The QR/toluene solution was mixed with an EVA/toluene solution, and the mixture was cast on a glass substrate. After drying in air, the composite polymer film was stretched in one direction and attached to a glass substrate. For orange-QRs, the obtained orange-QR/EVA 1D-stretched film showed good transparency, orange-colored strong luminescence under UV light, and different luminescence intensities under a linear polarizer placed parallel and perpendicular to the stretching direction (Fig. 3a). Similar results were observed for the yellow- and red-QR/EVA stretched films (Fig. S6, ESI†). These results indicated that the obtained 1D-stretched composite films showed yellow-, orange-, and red-colored PL with strong linear polarization sufficient to be detected by the naked eye using a linear polarizer.

For detailed evaluation of the 1D-stretched QR/EVA composite films, the effect of the stretching ratio on the degree of linear polarization in photoluminescence was first studied. Fig. 3b and c shows the angular dependencies of PL intensities at the highest peak (λ_{max}) before and after 1D stretching of QR/EVA composite films. The unstretched film showed no significant angular dependence on the PL intensity, while the 1D-stretched film showed maximum values at 0° and 180°, and minimum values at 90° and 270°. The degree of linear polarization in photoluminescence ($P_{LP\text{-}lum}$) was calculated using the following equation:

$$P_{LP} = \frac{I_{\parallel} - I_{\perp}}{I_{\parallel} + I_{\perp}} \quad (1)$$

where $I_{\parallel}$ and $I_{\perp}$ are the PL intensities of parallel and perpendicular components under depolarized excitation at 450 nm. Fig. 3d shows the correlation between the $P_{\text{LP-lum}}$ value and the 1D stretching ratio. The $P_{\text{LP-lum}}$ value increased almost linearly to the maximum value (0.68) upon 1D stretching up to six times. Further stretching showed no significant enhancement of the $P_{\text{LP-lum}}$ value. The orientation of QRs incorporated into the composite films was evaluated by TEM observation. As shown in Fig. 3e, 1D stretching provided 1D orientation of QRs in polymer media, whereas random orientation of QRs was confirmed in the unstretched polymer media (Fig. S8, ESI†).

To further investigate the linear polarization properties of 1D-stretched QR/EVA composite films, the degree of linear polarization in the absorption process ($P_{\text{LP-Abs}}$) was studied. The $P_{\text{LP-Abs}}$ value was calculated from PL intensities excited with parallel and perpendicular LP light at 450 nm (Fig. 4a). The obtained value ($P_{\text{LP-Abs}}$ = 0.28) was clearly smaller than the degree of linear polarization in PL ($P_{\text{LP-lum}}$ = 0.68, Fig. 4d). These results suggest that the fabricated LPL films play a role in efficiently converting unpolarized light into linearly polarized light, since they exhibit a small $P_{\text{LP-Abs}}$ value and a large $P_{\text{LP-lum}}$ value. These results also indicate that the mechanism of linear polarization generation differs between the absorption process ($P_{\text{LP-Abs}}$) and emission process ($P_{\text{LP-lum}}$), which is in good agreement with the mechanism reported previously.[12] In the absorption process, linear polarization mainly originates from the dielectric effect based on the morphological anisotropy of QRs.

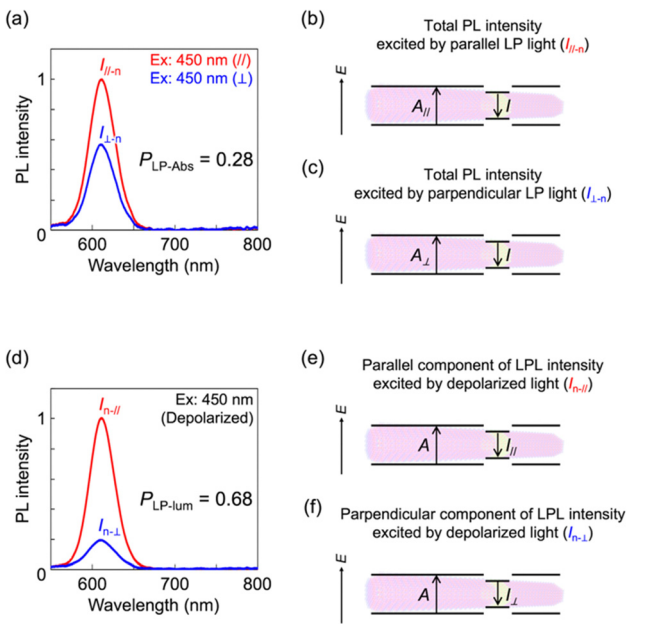

Fig. 4 (a) PL spectra of 1D stretched orange-QR/EVA composite films excited with parallel (red line) and perpendicular (blue line) LP light at 450 nm, respectively. (b and c) Schematic illustration of the study on generation of LP properties in the light absorption process. (d) LPL spectra of 1D stretched orange-QR/EVA composite films excited with depolarized light at 450 nm. Red and blue lines indicate parallel (∥) and perpendicular (⊥) LPL components against 1D stretching direction, respectively. (e and f) Schematic illustration of the study on generation of LP properties in the light emission process.

Namely, the rod-shaped CdS shell part mainly provides the linear polarization in the absorption process. In contrast, in the emission process, linear polarization is mainly derived from the quantum confinement effect based on the QR width being smaller than the exciton size. Indeed, the average widths of yellow-, orange-, and red-QRs were 4.6 nm, 4.9 nm, and 5.7 nm, respectively, which were sufficiently smaller than the exciton size (10.6–10.8 nm) calculated from the previously reported CdSe exciton Bohr radius (5.3–5.4 nm).[13]

To fabricate a luminescence-based CP convertor, a 1D stretched QR/EVA composite film was laminated with a quarter-wave plate where the fast axis was placed at −45° to the stretching direction (see ESI†). When the 1D-stretched film was directly laminated on a quarter-wave plate, a flexible-type luminescence-based CP convertor was prepared (Fig. S10, ESI†). When the PL was observed through a RH or LH circular polarizer, brighter light was observed through the LH circular polarizer. Quantitative evaluation of the RH- and LH-CP light components, as measured using a PL spectrometer with a CP light detection setup (see ESI†), confirmed that the total emission included 83% LH-CP light and 17% RH-CP light (Fig. 5a, left). The degree of circular polarization in the photoluminescence (P_{CP}) was calculated using the following equation:

$$P_{\text{CP}} = \frac{|I_{\text{LH}} - I_{\text{RH}}|}{I_{\text{LH}} + I_{\text{RH}}} \quad (2)$$

where I_{LH} and I_{RH} are the PL intensities of LH- and RH-CP light components under depolarized excitation at 450 nm, respectively. The obtained P_{CP} value (0.66) was similar to the $P_{\text{LP-lum}}$ value (0.68), proving that the polarization degree of LPL was directly converted to the polarization degree of CP light. Indeed, a good linear correlation between the P_{CP} values and $P_{\text{LP-lum}}$ values was observed as shown in Fig. 5d. The CP light produced by a luminescence-based CP convertor is not CPL but polarization-converted LPL. Therefore, the degree of circular polarization in the photoluminescence from a CP convertor should not be evaluated by using the dissymmetry factor (g) calculated using the following equation:

$$g = \frac{2(I_{\text{LH}} - I_{\text{RH}})}{I_{\text{LH}} + I_{\text{RH}}} \quad (3)$$

If we dare to calculate the $|g|$ value for comparing with that of CPL, the obtained P_{CP} value (0.66) corresponds to a $|g|$ value of 1.32. Interestingly, the sign of CP light could be switched with retention of the PL spectral pattern and intensity by simply changing the angle between the fast axis of the quarter-wave plate and stretching direction of the LPL films from +45° to −45° (Fig. 5a, right). Large P_{CP} values and switchable properties detectable by the naked eye were also observed from yellow- and red-colored CP convertors (Fig. 5b and c), although the P_{CP} values of yellow-colored CP convertors ($P_{\text{L-CP}}$ = 0.46 and $P_{\text{R-CP}}$ = 0.49) were relatively smaller than those of the other convertors. The P_{CP} values were plotted against the aspect ratio of QRs, confirming a good correlation between them (Fig. S11, ESI†). Considering the sufficiently smaller QR width against the estimated exciton size, the different polarization degrees can

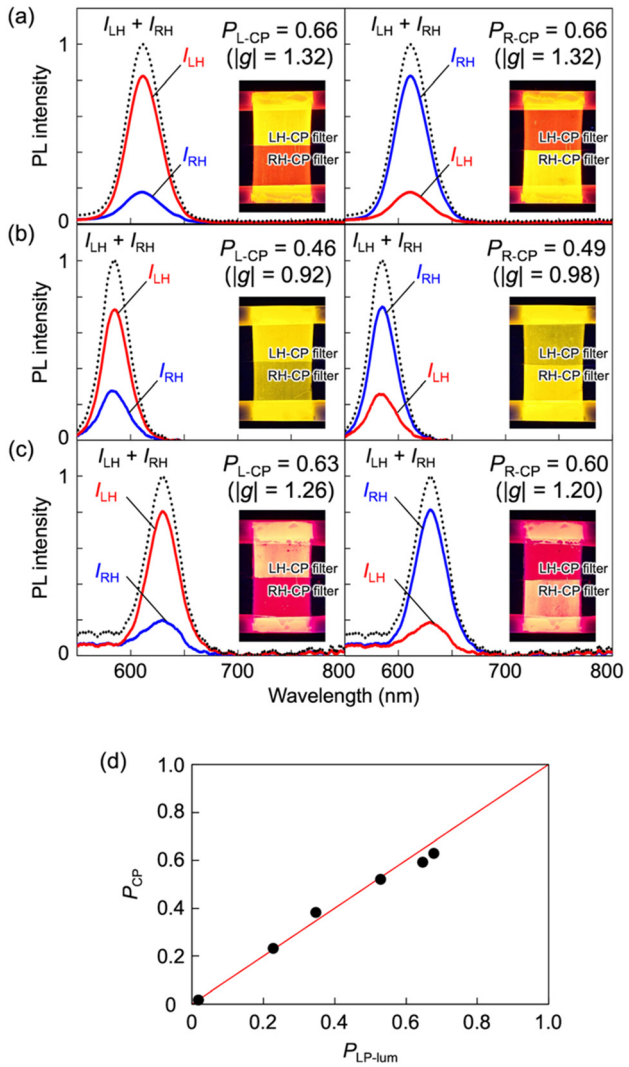

Fig. 5 PL spectra of (a) orange-, (b) yellow-, and (c) red- CP convertors. Excitation wavelength, 450 nm. All the spectra on the left (or right) were obtained from LH- (or RH-) CP convertors, respectively. LH- and RH-CP light components in the PL were measured using a photodetector with a CP light detection optical setup (see ESI†). Insets are photographs of (a) orange-, (b) yellow-, and (c) red- LH- (left) and RH- (right) CP convertors under UV light at 365 nm. Luminescence of these CP convertors was observed through LH- and RH-CP filters. (d) Correlation between the $P_{LP\text{-}lum}$ and P_{CP} values. The red line is the theoretical curve.

be explained from the different orientations of the QRs in the polymer media which might correspond to the aspect ratio of QRs.

A unique advantage of the CP convertor was observed when a linear polarizer was combined with it. When a linear polarizer was placed between the LPL film and quarter-wave plate, almost completely single-handed CP light ($P_{CP} > 0.95$) was produced because the perpendicular component of emitted light was almost perfectly cut off. If the $P_{LP\text{-}lum}$ value of an LPL film is maximum ($P_{LP\text{-}lum} = 1$), the light intensity of transmitted light from the total PL intensity, defined as the light-extraction efficiency (η_{LEE}), will be 100% in theory. In contrast, the light-extraction efficiency of nonpolarized PL will

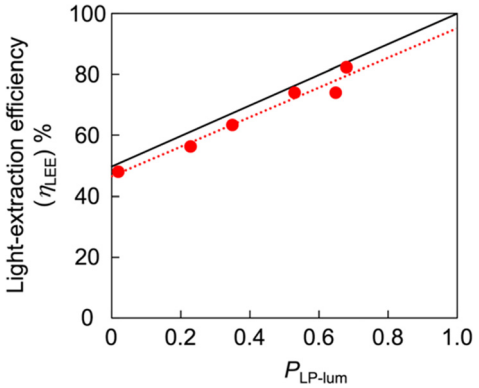

Fig. 6 Correlation between the P_{CP} and η_{LEE} values. Red plots are experimentally obtained data and red dotted line is approximation curve. Each η_{LEE} value of experimental data was calculated from $I_{with\text{-}LP}/I_{without\text{-}LP}$, where $I_{with\text{-}LP}$ and $I_{without\text{-}LP}$ are PL intensities at λ_{max} detected with and without a linear polarizer. The black line is the theoretical curve when the a_{loss} value is 1.

ideally be 50%. Linear correlation between the η_{LEE} value and $P_{LP\text{-}lum}$ value was observed, as summarized in the following equation:

$$\eta_{LEE} = \frac{I_{CP}}{I_{total}} = \left(\frac{1}{2} + \frac{P_{LP-lum}}{2}\right) \times a_{loss} \times 100 \qquad (4)$$

where I_{total} is the total PL intensity, I_{CP} is light intensity of the LH- or RH-CP light component, and factor a_{loss} is the loss coefficient including light scattering. The experimental data, indicated as red dots in Fig. 6, show a linear but slightly lower line compared with the theoretical line. This lowering might be explained from light scattering effects at the interface owing to the refractive index mismatch. Interestingly, this correlation curve indicates that a high light-extraction efficiency (η_{LEE}) and high polarization degree ($P_{LP\text{-}lum}$, namely P_{CP}) can be achieved at the same time. At this point, the luminescence-based CP

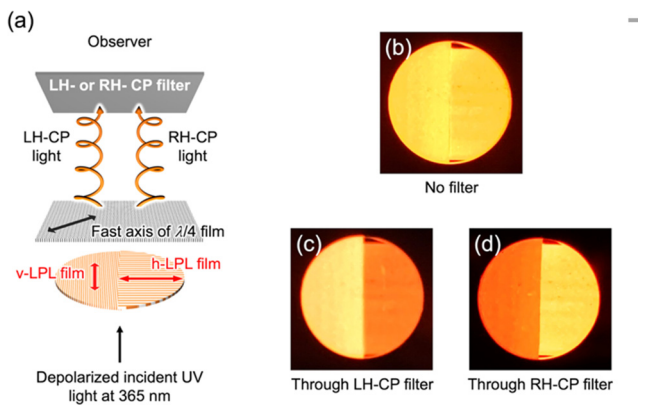

Fig. 7 (a) Schematic illustration of a parallel-type luminescence-based CP convertor. LH- and RH-CP light were generated by patterning of LPL, and detected by the naked eye using a circular polarizer. (b–d) Photographs of a parallel-type luminescence-based CP convertor composed of a v-LPL film on the left and a h-LPL film on the right under UV light at 365 nm. Luminescence was observed (b) without a filter, or using (c) LH-CP and (d) RH-CP filters.

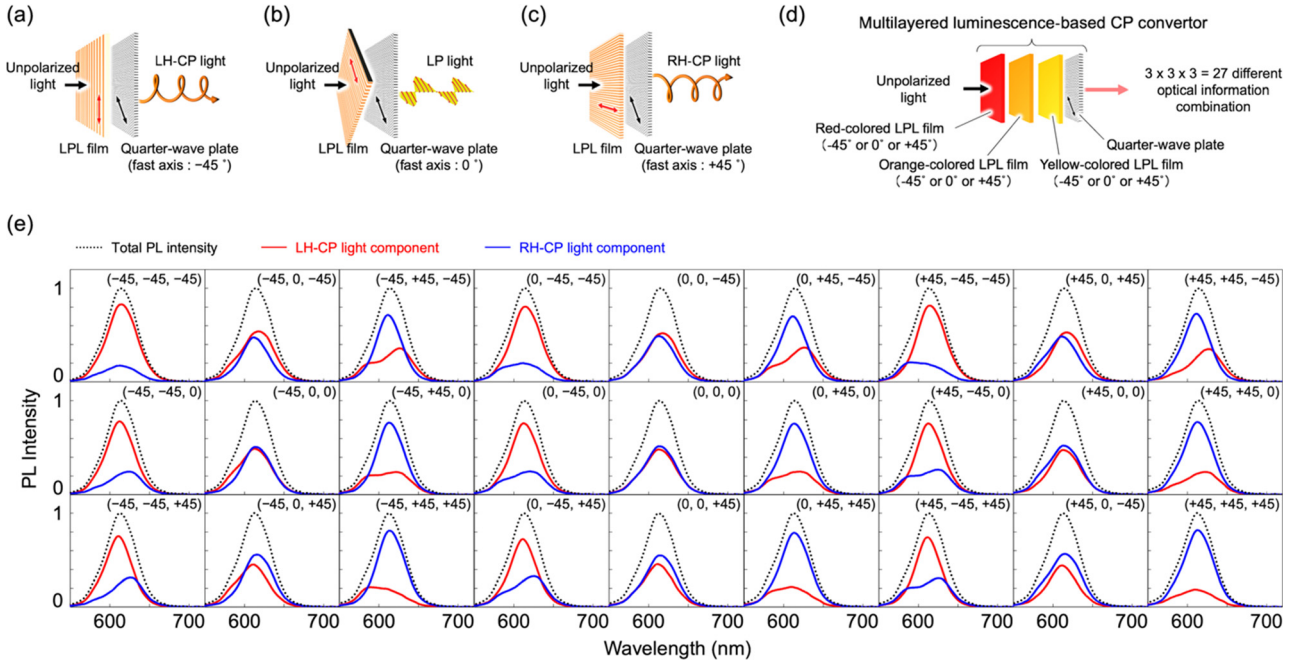

Fig. 8 Schematic illustration of a luminescence-based CP convertor with angles between the polarization plane of the LPL film and fast axis of the quarter-wave plate of (a) −45°, (b) 0°, and (c) +45°. (d) Schematic illustration of a multi-layered luminescence-based CP convertor. (e) Twenty-seven different pieces of optical information from a three-layered luminescence-based CP convertor. Inside the parentheses each angle between the polarization plane of the red- (left), orange- (middle), and yellow-colored (right) LPL films and fast axis of the quarter-wave plate, respectively, is indicated. Excitation wavelength, 450 nm.

convertor is considered as totally different from that of the other methods. For example, even in the case of imperfectly optimized results of the current study, the prepared CP convertor, which is composed of high quantum yield QRs (approximately 60–70%[12a]), can produce high-purity CP light (P_{CP} = 96%) with high light-extraction efficiency (η_{LEE} = 82%).

The luminescence-based CP convertor composed of several LPL films made a significant contribution in multiplexing optical information. The first example was observed in the parallel arrangement of LPL films with the same PL spectral pattern. As shown in Fig. 7a, the QR/EVA composite film stretched vertically (v-LPL film) was placed on the left side, and another film stretched horizontally (h-LPL film) was placed on the right side. When the fast axis of the quarter-wave plate was adjusted to be at +45° in the vertical direction and at −45° in the horizontal direction, the CP convertor produced LH-CP light on the left side and RH-CP light on the right side. Although the difference in CP-light handedness was not detectable by the naked eye alone, the use of LH- and RH-CP filters allowed clear observation by the naked eye, as shown in Fig. 7b–d. These results indicated that the luminescence-based CP conversion approach enabled multiplex optical anisotropy by patterning the orientation of LPL generating agents.

The second example was observed in multi-layered LPL films exhibiting different PL colors. When the angles between the polarization plane of the LPL film and fast axis of the quarter-wave plate were −45°, 0°, and +45°, LH-CP, parallel LP, and RH-CP light were produced, as shown in Fig. 8a–c, respectively. Taking advantage of this, further multiplexing of the optical information was demonstrated by laminating different color-emitting LPL films at different angles between the polarization plane of the LPL film and the fast axis of the quarter-wave plate. To the best of our knowledge, this is the first time that such a multi-layer LPL film system has been fabricated and investigated. When the yellow-, orange-, and red-color-emitting LPL films were laminated at three different angles (−45°, 0°, and +45°) against the fast axis of the quarter-wave plate, 27 possible pieces of optical information were estimated to be produced, as shown in Fig. 8d. By measuring PL spectra of all combinations, we confirmed that 27 different pieces of optical information, as combinations of wavelength, PL intensity, and polarization, were produced from a three-layered luminescence-based CP convertor by only selecting the angle (Fig. 8e). Interestingly, the difference between these 27 pieces of optical information was not clearly detected by the naked eye using CP filters (Fig. S12, ESI†), in contrast to the parallel-type CP convertor (Fig. 7). These results indicate that the multi-layered luminescence-based CP convertor has potential for use in high-level security printing.

Conclusions

We have reported the first example of the generation of high-purity CP light with high light intensity based on a luminescence-based CP convertor composed of an LPL film and a quarter-wave plate. The synthesized yellow-, orange-, and red-QRs showed significant LPL when oriented by 1D stretching

of the composite polymer films. After lamination of these LPL films with a quarter-wave plate, LPL was effectively converted to high-purity CP light with retention of the PL spectral pattern, light intensity, and the large degree of polarization (*e.g.*, P_{CP} = 0.66, which corresponds to $|g_{lum}|$ = 1.32). The sign of CP light was easily switched by simply changing the angle between the fast axis of the quarter-wave plate and the polarization plane of LPL from +45° to −45° (or from −45° to +45°). Completely single-handed CP light (P_{CP}, ∼0.95) was also produced when a linear polarizer was placed between the LPL film and quarter-wave plate owing to almost perfect cutting-off of the perpendicular component of emitted light. The equations obtained from both theoretical and experimental studies indicated that a high light-extraction efficiency (η_{LEE}) and a high polarization degree ($P_{LP\text{-}lum}$, namely P_{CP}) can be achieved at the same time. At this point, the luminescence-based CP convertor is totally different from the other CP convertors. Furthermore, we also demonstrate the first example of parallel-type and multi-layered luminescence-based CP light convertors for multiplexing of optical information. These findings will help designing next-generation CP light-generating materials for various fields, including photoelectric conversion, plant factory, and security printing.

Author contributions

Y. Okazaki designed the project, raised funds, and wrote the original draft. All the experimental measurements, observation, analysis were carried out by Y. Okazaki and M. Kimura with equal contribution. T. Sagawa assisted the synthesis of various quantum rods and its analysis. K. Hachiya assisted the mechanistic consideration of the origin of linear polarization in the light absorption and emission processes. All authors discussed the results and contributed to the interpretation of the data.

Conflicts of interest

There are no conflicts to declare.

Acknowledgements

This work was supported by JSPS KAKENHI (grant number 19K15376 and 20KK0122), SPIRITS2020 from Kyoto University, the Kansai Research Foundation for Technology Platform, and the Masuyakinen Basic Research Foundation. We are grateful to T. Kiyomura from the Institute for Chemical Research, Kyoto University for TEM, HRTEM, and STEM-EDX observation, which was supported by Kyoto University Nano Technology Hub in the Nanotechnology Platform Project sponsored by the Ministry of Education, Culture, Sports, Science and Technology (MEXT), Japan (grant numbers JPMXP09A21KT0014, and JPMXP1222KT0001).

Notes and references

1 (*a*) G. Iftime, F. L. Labarthet, A. Natansohn and P. Rochon, *J. Am. Chem. Soc.*, 2000, **122**, 12646–12650; (*b*) Y. Wang, T. Sakamoto and T. Nakano, *Chem. Commun.*, 2014, **48**, 1871–1873; (*c*) T. Nakano, *Chem. Rec.*, 2014, **14**, 369–385; (*d*) M. Fujiki, Y. Donguri, Y. Zhao, A. Nakao, N. Suzuki, K. Yoshida and W. Zhang, *Polym. Chem.*, 2015, **6**, 1627–1638.

2 (*a*) T. Manaka, H. Kon, Y. Ohshima, G. Zou and M. Iwamoto, *Chem. Lett.*, 2006, **35**, 1028–1029; (*b*) S.-T. Wu, Z.-W. Cai, Q.-Y. Ye, C.-H. Weng, X.-H. Huang, X.-L. Hu, C.-C. Huang and N.-F. Zhuang, *Angew. Chem., Int. Ed.*, 2014, **53**, 12860–12864; (*c*) M. Miyata, M. Teraguchi, H. Endo, T. Kaneko and T. Aoki, *Chem. Lett.*, 2014, **43**, 1476–1477.

3 (*a*) G. C. McLeod, *Limnol. Oceanogr.*, 1957, **7**, 360–362; (*b*) P. P. Shibaye and R. G. Pergolizzi, *Int. J. Bot.*, 2011, **7**, 113–117; (*c*) E. Lkhamkhuu, K. Zikihara, H. Katsura, S. Tokutomi, T. Hosokawa, Y. Usami, M. Ichihashi, J. Yamaguchi and K. Monde, *Plant Biotechnol.*, 2020, **37**, 57–67.

4 (*a*) J. Gilot, R. Abbel, G. Lakhwani, E. W. Meijer, A. P. H. J. Schenning and S. C. J. Meskers, *Adv. Mater.*, 2010, **22**, E131–E134; (*b*) W. Qin, H. Xu and B. Hu, *ACS Photonics*, 2017, **4**, 2821–2827; (*c*) M. Wei, X. Hao, A. B. Saxena, W. Qin and S. Xie, *J. Phys. Chem. C*, 2018, **122**, 12566–12571.

5 (*a*) S. H. Chen, D. Katsis, A. W. Schmid, J. C. Mastrangelo, T. Tsutsui and T. N. Blanton, *Nature*, 1999, **397**, 506–5084; (*b*) H.-J. Lee, B. R. Lee, S.-W. Choi and M. H. Song, *Opt. Express*, 2012, **20**, 24473–24481; (*c*) S. Furumi, *Poly. J.*, 2013, **45**, 579–593; Y. Nagata, K. Takagi and M. Suginome, *J. Am. Chem. Soc.*, 2014, **136**, 9858–9861; (*d*) K. Akagi, *Bull. Chem. Soc. Jpn.*, 2019, **92**, 1509–1655.

6 (*a*) E. M. Sánchez-Carnerero, A. R. Agarrabeitia, F. Moreno, B. L. Maroto, G. Muller, M. J. Ortiz and S. de la Moya, *Chem. – Eur. J.*, 2015, **21**, 13488–13500; (*b*) J. Kumar, T. Nakashima and T. Kawai, *J. Phys. Chem. Lett.*, 2015, **6**, 3445–3452; (*c*) Y. Sang, J. Han, T. Zhao, P. Duan and M. Liu, *Adv. Mater.*, 2020, **32**, 1900110; (*d*) G. Albano, G. Pescitelli and L. Di Bari, *Chem. Rev.*, 2020, **120**, 10145–10243; (*e*) S. Jiang and N. A. Kotov, *Adv. Mater.*, 2022, 2108431.

7 (*a*) A. C. Neville and S. Caveney, *Biol. Rev.*, 1969, **44**, 531–562; (*b*) D. J. Brink, N. G. van der Berg, L. C. Prinsloo and I. J. Hodgkinson, *J. Phys. D: Appl. Phys.*, 2007, **40**, 2189–2196; (*c*) S. A. Jewell, P. Vukusic and N. W. Roberts, *New J. Phys.*, 2007, **9**, 99; (*d*) T.-H. Chiou, S. Kleinlogel, T. Cronin, R. Caldwell, B. Loeffler, A. Siddiqi, A. Goldizen and J. Marshall, *Curr. Biol.*, 2008, **18**, 429–434; (*e*) S. Vignolini, P. J. Rudall, A. V. Rowland, A. Reed, E. Moyroud, R. B. Faden, J. J. Baumberg, B. J. Glover and U. Steiner, *Proc. Natl. Acad. Sci. U. S. A.*, 2012, **109**, 15712–15715.

8 (*a*) P. M. L. Block and H. P. J. M. Dekkers, *Chem. Phys. Lett.*, 1989, **161**, 188–194; (*b*) Y. Nagata and T. Mori, *Front. Chem.*, 2020, **8**, 448; (*c*) L. Arrico, L. Di Bari and F. Zinna, *Chem. – Eur. J.*, 2021, **27**, 2920–2934.

9 (*a*) P. D. Cunningham, J. B. Souza Jr., I. Fedin, C. She, B. Lee and D. V. Talapin, *ACS Nano*, 2016, **10**, 5769–5781; (*b*) A. Chakrabarty, G. Raffy, M. Maity, L. Gartzia-Rivero, S. Marre, C. Aymonier, U. Maitra and A. D. Guerzo, *Small*, 2018, **14**, 1802311; (*c*) Y. Sagara, A. Seki, Y. Kim and N. Tamaoki, *J. Mater. Chem. C*, 2018, **6**, 8453–8459; (*d*) J. Koo, S.-I. Lim, S. H. Lee, J. S. Kim, Y.-T. Yu, C.-R. Lee, D.-Y. Kim and K.-U. Jeong, *Macromolecules*, 2019, **52**, 1739–1745; (*e*) L. Tao, K. Lan, C.-L. Zhong, Y.-J. Zhou, P. Wang, F. Fan, Z. Shen and H.-L. Xie, *J. Mater. Chem. C*, 2020, **8**, 16561–16568; (*f*) R. A. M. Hikmet, P. T. K. Chin, D. V. Talapin and H. Weller, *Adv. Mater.*, 2005, **17**, 1436–1439; (*g*) Z. Zhou, H. Liu, W. Zhang, Z. Wen, J. Hao, B. Xu, K. Wang, K.-L. Teo and X.-W. Sun, *IEEE J. Quantum Electron.*, 2019, **55**, 710026; (*h*) H. He, J. Liu, K. Li, Z. Yin, J. Wang, D. Luo and Y. J. Liu, *Nano Lett.*, 2020, **20**, 4204–4210; (*i*) A. Rizzo, C. Nobile, M. Mazzeo, M. D. Giorgi, A. Fiore, L. Carbone, R. Cingolani, L. Manna and G. Gigli, *ACS Nano*, 2009, **3**, 1506–1512; (*j*) K. Yoshihara, M. Yamanaka, S. Kanno, S. Mizushima, J. Tsuchiyagaito, K. Kondo, T. Kondo, D. Iwasawa, H. Komiya, A. Saso, S. Kawaguchi, K. Goto, S. Ogata, H. Takahashi, A. Ishii and M. Hasegawa, *New J. Chem.*, 2019, **43**, 6472–6479; (*k*) S. Kaur, G. Murali, R. Manda, Y. C. Chae, M. Yun, J. H. Lee and S. H. Lee, *Adv. Opt. Mater.*, 2018, **6**, 1800235; (*l*) T. Du, J. Schneider, A. K. Srivastava, A. S. Sucha, V. G. Chigrinov., H. S. Kwok and A. L. Rogachi, *ACS Nano*, 2015, **9**, 11049–11055; (*m*) K. Hisano, M. Aizawa, M. Ishizu, Y. Kurata, W. Nakano, N. Akamatsu, C. J. Barrett and A. Shishido, *Sci. Adv.*, 2017, **3**, e1701610; (*n*) W. Zhang, J. Schneider, V. G. Chigrinov, H. S. Kwok, A. L. Rogach and A. K. Srivastava, *Adv. Opt. Mater.*, 2018, **6**, 1800250.

10 (*a*) L. Carbone, C. Nobile, M. De Giorgi, F. D. Sala, G. Morello, P. Pompa, M. Hytch, E. Snoeck, A. Fiore, I. R. Franchini, M. Nadasan, A. F. Silvestre, L. Chiodo, S. Kudera, R. Cingolani, R. Krahne and L. Manna, *Nano Lett.*, 2007, **7**, 2942–2950; (*b*) J. Dehnel, Y. Barak, I. Meir, A. K. Budniak, A. P. Nagvenkar, D. R. Gamelin and E. Lifshitz, *ACS Nano*, 2020, **14**, 13478–13490.

11 S. Kumar and T. Nann, *Small*, 2006, **2**, 316–329.

12 (*a*) D. V. Talapin, R. Koeppe, S. Gotzinger, A. Kornowski, J. M. Lupton, A. L. Rogach, O. Benson, J. Feldmann and H. Weller, *Nano Lett.*, 2003, **3**, 1677–1681; (*b*) A. Sitt, A. Salant, G. Menagen and U. Banin, *Nano Lett.*, 2011, **11**, 2054–2060; (*c*) J. S. Kamal, R. Gomes, Z. Hens, M. Karvar, K. Neyts, S. Compernolle and F. Vanhaecke, *Phys. Rev. B: Condens. Matter Mater. Phys.*, 2012, **85**, 035126; (*d*) I. Hadar, G. B. Hitin, A. Sitt, A. Faust and U. Banin, *J. Phys. Chem. Lett.*, 2013, **4**, 502–507; (*e*) Y. Ge, M. Zhang, L. Wang, L. Meng, J. Tang, Y. Chen, L. Wang and H. Zhong, *Adv. Opt. Mater.*, 2019, **7**, 1900330.

13 (*a*) K. Kyhm, J. H. Kim, S. M. Kim and H. Yang, *Opt. Mater.*, 2007, **30**, 158–160; (*b*) V. Babentsov and F. Sizov, *Opto-Electron. Rev.*, 2008, **16**, 208–225.

